Clockwise-directional circle swimmer moves counter-clockwise in Petri dish- and ring-like confinements†

Sven van Teeffelen,* Urs Zimmermann and Hartmut Löwen

A self-propelled rod which is driven by a constant internal force and torque performs circular motion in two spatial dimensions with an "internal" radius governed by the torque-to-force ratio and is referred to as a circle swimmer. Using analytical methods and computer simulations, we study the Brownian dynamics of a circle swimmer in a confining Petri dish- or ring-shaped geometry and compute the mean of the swimmer's position, its steady-state properties and its orientational motion. For small torque-to-force ratios, the confinement inverts the orientational sense of the motion: a clockwise-directional circle swimmer moves counter-clockwise in the confinement. Our results are verifiable for self-propelled colloidal rods, for vibrated granular rods and for motile bacteria in cylindrical confinements.

I. Introduction

There are quite different examples of self-propelled ("active") particles[1–3] which move in circles in two dimensions rather than along a straight line. When confined to a planar substrate, certain bacteria[4–9] and spermatozoa[10–12] swim in circles. Spherical camphors have been shown to swim in circles if confined to an air–water interface.[13] Furthermore it is possible to prepare catalytically driven nanorods[14–16] and colloidal particles[17] with a tilted motor which will result in circular motion of the particles. The effect of confinement on catalytically driven particles has recently been studied by Popescu *et al.*[18] Next, a vibrated polar granular rod[19] on a planar substrate with an additional left–right asymmetry will move along circles. Finally, the trajectories of deformable particles[20] and even of completely blinded and ear-plugged pedestrians can possess significant circular characteristics.[21]

The effect of planar confining walls on swimming particles or organisms in three dimensions has been studied in detail by Elgeti and Gompper for the case of a model system consisting of a self-propelled rod[22] and by Li *et al.*[23] and Berke *et al.*[24] for the case of self-propelled bacteria. It is further possible to confine motile particles into various kinds of additional lateral confinement ranging from linear microfluidic channels of desired geometry[25] to finite circular confinements.[19,26] A detailed knowledge about the dynamics of self-propelled particles in confinement is crucial for the fabrication of switching devices for active particles which rectify,[27] filter and sort out[25] various self-propelled particles. These devices open up challenging applications to steer the dynamical behaviour of active soft matter.

Recently we have modelled an active particle performing circular motion by a Brownian rod which experiences an internal force along its orientation and a constant torque.[28] In the absence of any thermal fluctuations, this circle swimmer moves on a circle with an "internal" radius that is inversely proportional to the torque-to-force ratio. Thermal fluctuations smear out this circular motion leading to diffusive long-time dynamics. For linear channel geometries, it was shown[28] that the long-time motion of a Brownian circle swimmer is maximal for an optimal torque-to-force ratio.

In this paper we study this model of a Brownian circle swimmer in circular confinement with Petri dish- and ring-like geometries. In particular, one can expect a competition of the two length scales set by the radius of the confinement and the "internal" radius of the circular motion. One key dynamical property important for the construction of devices is whether the particles rotates on average clockwise or counter-clockwise in a confining ring. Since the clockwise–counter-clockwise symmetry of the ring is broken by the intrinsic circular motion, there is a nontrivial long-time limit leading either to clockwise or counter-clockwise rotation. By using extensive Brownian dynamics computer simulations and an analytical theory for a wall-induced sliding mode, we show here that the confinement inverts the orientational sense of the particle rotation provided the torque-to-force ratio is small enough. In this case, a clockwise-directional circle swimmer moves counter-clockwise in the confinement. For the actual rotational sense, thermal fluctuations play a crucial role. The predicted inversion from clockwise to counter-clockwise motion can in principle be verified in a number of possible experimental set-ups for two-dimensional circle swimmers in confinement.

The paper is organized as follows: in section II we introduce the model and summarize the dynamical behaviour of a circle swimmer in the bulk. In section III, we summarize analytical results for the sliding mode and present simulation data in section IV. In particular, we discuss the noise-averaged trajectories of the swimmer, its radially-resolved probability distributions and finally its sense of rotation in the ring. We conclude in section V by discussing realisations of our model for various circle-swimming systems.

II. The model

The Brownian swimmer under consideration, which was already introduced in ref. 28, is modelled as a rod-like colloidal particle

Institut für Theoretische Physik II: Weiche Materie, Heinrich-Heine-Universität Düsseldorf, Universitätsstraße 1, D-40225 Düsseldorf, Germany. E-mail: teeffelen@thphy.uni-duesseldorf.de
† This paper is part of a *Soft Matter* themed issue on Modelling of soft matter. Guest editor: Mark Wilson.

of length L and width d. Neglecting hydrodynamic interactions with the confining walls, its overdamped motion in two dimensions is governed by the Langevin equations for the rod center-of-mass position

$$\dot{\mathbf{r}} = \beta\mathbf{D}\cdot[F\hat{\mathbf{u}} - \nabla V(\mathbf{r},\phi) + \mathbf{f}] \quad (1)$$

and for the rod orientation

$$\dot{\phi} = \beta D_r[M - \partial_\phi V(\mathbf{r},\phi) + \tau] , \quad (2)$$

respectively, where dots denote time derivatives and $\beta^{-1} = k_B T$ is the thermal energy. The angle ϕ denotes the swimmer's orientation with respect to the x-axis, as sketched in Fig. 1. The rod's short time diffusion tensor

$$\mathbf{D} = D_\parallel(\hat{\mathbf{u}} \otimes \hat{\mathbf{u}}) + D_\perp(\mathbf{I} - \hat{\mathbf{u}} \otimes \hat{\mathbf{u}}) \quad (3)$$

is given in terms of the short time longitudinal ($D_\parallel$) and transverse ($D_\perp$) translational diffusion constants, with the orientation vector $\hat{\mathbf{u}} = (\cos\phi, \sin\phi)$, $\mathbf{I}$ the unit tensor and $\otimes$ a dyadic product. D_r is the short time rotational diffusion constant. $F\hat{\mathbf{u}}$ is a constant *effective* force that represents the internal propulsion mechanism responsible for the deterministic motion in the rod orientation, and M is a constant *effective* torque, originating from the internal propulsion mechanism or from an external field, which yields the deterministic circular motion (see the sketch in Fig. 1). $V(\mathbf{r}, \phi)$ is an external confining potential. $\mathbf{f}$ and τ are the zero mean Gaussian white noise random force and random torque originating from the solvent, respectively. Their variances are given by

$$\overline{f_\parallel(t)f_\parallel(t')} = 2\delta(t - t')/(\beta^2 D_\parallel),$$
$$\overline{f_\perp(t)f_\perp(t')} = 2\delta(t - t')/(\beta^2 D_\perp),$$
$$\overline{\tau(t)\tau(t')} = 2\delta(t - t')/(\beta^2 D_r), \quad (4)$$

where $f_\parallel, f_\perp$ are the components of $\mathbf{f}$ parallel and perpendicular to $\hat{\mathbf{u}}$, respectively. The bars over the quantities denote a noise average. Henceforth, we consider a very thin rod of length $L \gg d$, for which the short-time diffusion constants in the three-dimensional bulk are given by $D_r/D_\parallel = 3/(2L^2)$, $D_\perp = D_\parallel/2$. We
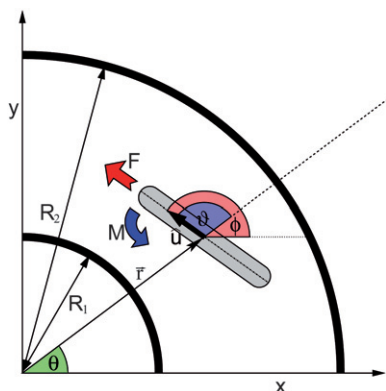

Fig. 1 Sketch of the swimmer in ring-like confinement. Indicated are the rod center-of-mass position in polar coordinates $\mathbf{r} = (r, \theta)$, the rod orientation ϕ, and the relative orientation with respect to the wall, $\vartheta = \phi - \theta$. The swimmer is confined to a ring of dimensions $R_1 < r < R_2$. The propelling force F and the torque M are also indicated.

will denote all times in units of $\tau_B = L^2/D_\parallel$, lengths in units of L, and energies in units of β^{-1}. As already pointed out in ref. 28, F and M are *effective* net forces that could be determined in the bulk from the forward and angular velocities $F = |\dot{\mathbf{r}}|/(\beta D_\parallel)$ and $M = |\dot{\phi}|/(\beta D_r)$, respectively, but are not necessarily directly connected to the internal propulsion mechanism.[29] The propulsion velocities have been calculated including full hydrodynamics for a set of simple model swimmers, which are, *e.g.*, driven by chemical reactions[30,18] or by the combined motion of three connected spheres.[31]

Next, we introduce a circular, ring-like potential of purely repulsive walls, which confines the swimmer's motion to a ring of dimensions $R_1 < r < R_2$, where $r = |\mathbf{r}|$ is the radial coordinate of the swimmer's center-of-mass position. For simplicity, we model the confinement by an integrated segment-wall power-law potential in the radial direction,

$$V(r, \vartheta) = \int_{-\frac{L}{2}}^{\frac{L}{2}} v(r, l, \vartheta)\mathrm{d}l , \quad (5)$$

where $\vartheta = \phi - \theta$ is the difference between the angular coordinate of the swimmer's center-of-mass position θ and its orientation ϕ, *i.e.*, ϑ is the relative angle of the swimmer's center of mass with respect to the closest point on either of the two confining walls (see Fig. 1). The segment-wall potential of the rod segment at the position l along the contour is given by

$$v(r, l, \vartheta) = (\beta L)^{-1}\left\{ \left|\frac{L}{R_1 - \sqrt{r^2 + l^2 + 2rl\cos\vartheta}}\right|^n \right.$$
$$\left. + \left|\frac{L}{R_2 - \sqrt{r^2 + l^2 + 2rl\cos\vartheta}}\right|^n \right\}, \quad (6)$$

if the rod segment is situated between the two walls, *i.e.*, if $R_1^2 < r^2 + l^2 + 2rl\cos\vartheta < R_2^2$, and infinite otherwise. n is a large exponent, which is assumed infinite in our analytical studies and set equal to $n = 6$ in the Brownian dynamics computer simulations further down. In the limit of large radii $R_1, R_2 \gg L$, which we assume in the following, the potential simplifies to the expression

$$v(r, l, \vartheta) \simeq (\beta L)^{-1}\left\{ \left|\frac{L}{R_1 - r + l\cos\vartheta}\right|^n \right.$$
$$\left. + \left|\frac{L}{R_2 - r + l\cos\vartheta}\right|^n \right\}, \quad (7)$$

which yields

$$V(r, \vartheta) \simeq \frac{L^{n-1}}{\beta(n-1)\cos\vartheta}\left\{ \left|(R_1 - r + (L/2)\cos\vartheta)^{-(n-1)}\right.\right.$$
$$\left. - (R_1 - r - (L/2)\cos\vartheta)^{-(n-1)}\right|$$
$$+ \left|(R_2 - r + (L/2)\cos\vartheta)^{-(n-1)} - (R_2 - r - (L/2)\cos\vartheta)^{-(n-1)}\right|\right\}. \quad (8)$$

We consider two qualitatively different situations: The radius of the inner wall R_1 is either zero or finite. The former case yields

a circular, Petri dish-like confinement with a single outer wall, whereas the latter case yields the described ring-like confinement with an inner and an outer wall.

In this final paragraph we shortly comment on the effect of hydrodynamic interactions between the swimmer and the confining walls, which depends on the specific experimental realisation of our model. The hydrodynamics of a bacterium being confined between two parallel glass plates in three dimensions has been studied in detail by Berke *et al.*[24] A simplified model system of a self-propelled rod between two plates was studied by Elgeti and Gompper.[22] In our model, as we are only interested in the motion in the two-dimensional plane, those effects are captured by the short-time diffusion tensor. The effect of the additional laterally confining walls deserves additional discussion. First, if the wall potential only affects the swimmer position and orientation but not the solvent, hydrodynamic interactions can be ignored. Such a setup could be achieved by applying a laser tweezing potential to an autocatalytic colloidal realization of a circle swimmer. However, to our knowledge, an attempt to confine self-propelled colloids with the help of a laser tweezer has not been pursued yet. On the contrary, in case the solvent is confined as well, hydrodynamic interactions between the swimmer and the wall lead in principle to an *r*-dependent diffusion tensor,[18,32] which is ignored in our model. In order to take hydrodynamic interactions into account, knowledge about the precise nature of the wall, of the particle shape, of the propulsion mechanism, and of the confinement in the *z*-direction perpendicular to the *xy*-plane is necessary. Since we do not specify these details in our model we can only refer to the respective (not yet realized) experiments (*cf.* the Conclusions).

III. Deterministic steady-state motion in the noise-free case

Before considering the stochastic motion of the swimmer in confinement, we present here the deterministic motion in the case of no thermal noise present. At first, we briefly recall the properties of the free swimmer, which serves as a reference point, *i.e.*, we set $V(\mathbf{r}, \phi) = 0$. In this simplest situation, the rod center of mass describes a perfect circle of radius

$$R_0 = \frac{D_\parallel F}{D_r M} , \quad (9)$$

with the circular frequency

$$\omega_0 \equiv \dot\phi = \beta D_r M \quad (10)$$

which has the same sign as the internal torque M. In the presence of the ring-like confinement, however, this circular motion is disturbed and the swimmer eventually performs a steady-state *sliding motion* along the inner or outer wall, depending on whether the ratio $M/(LF)$ lies within an R_1- and R_2-dependent range and if the initial coordinates $\mathbf{r}_0 = \mathbf{r}(t = 0)$ and $\phi_0 = \phi(t = 0)$ are chosen appropriately. The following consideration is similar to the situation in a linear channel, which has been discussed in ref. 28. The sliding motion is characterized by a constant *r*-position close to one of the walls and by a constant relative angle ϑ of the rod orientation with respect to the wall. Making

use of the zero-noise versions of eqn (1) and (2) the steady-state coordinates are obtained as the solutions of the two conditions

$$\dot{r} = \beta \left\{ \mathbf{D} \cdot \left[F\hat{u} - \partial_r V(r, \vartheta)\hat{e}_r \right] \right\} \cdot \hat{e}_r = 0 ,$$
$$\dot{\vartheta} = \beta D_r \left[M - \partial_\vartheta V(r, \vartheta) \right] - \dot{\theta} = 0 , \quad (11)$$

where $\hat{\mathbf{e}}_r = (\cos\theta, \sin\theta)$ is the unit vector in radial direction and $\dot{\theta}$ is the yet unknown constant angular velocity at which the rod moves along the channel. The constancy of $\dot{\theta}$, in turn, implies that the angular velocity of the swimmer's orientation $\dot{\phi}$, which we refer to as spinning frequency henceforth, takes the same value $\dot{\phi} = \dot{\theta}$.

Without loss of generality, we consider the case $M > 0$, *i.e.*, the rod would rotate counter-clockwise in the bulk with a frequency $\omega_0 > 0$, according to eqn (10). During the steady state in confinement, however, the rod is hindered in its intrinsic motion by the presence of the walls, as is sketched in Fig. 2. In particular, if the rod performs its steady-state sliding motion at the outer wall, it might move in negative angular direction, $\dot{\theta} = \dot{\phi} < 0$, which implies an inversion of the spin in confinement as compared to the situation in the bulk, *i.e.*, $\dot{\phi} < 0$ whereas $\omega_0 > 0$.

In the following, we first discuss the situation in which the intrinsic radius of the swimmer is smaller than both the inner and the outer radii $R_0 < R_i$, $i = 1, 2$, *i.e.*, the torque-to-force ratio is assumed to obey $M/(LF) > (2/3)L/R_i$. The opposite case of $M/(LF) < (2/3)L/R_i$ is discussed further down. In the considered regime of intermediate torque-to-force ratios, counter-clockwise rotational motion with $\dot{\theta} = \dot{\phi} > 0$ does only persist if the rod is situated in the sliding mode at the inner wall. At the outer wall, on the contrary, the rod slides in negative angular direction, $\dot{\theta} = \dot{\phi} < 0$. In the limit of hard walls ($n \to \infty$), the solutions to the steady-state conditions (11) simplify to the real-valued roots $\cos\vartheta_\alpha$ of a sixth-order polynomial in $\cos\vartheta$, where the index α refers to the different–yet to be determined–solutions. Equivalently, the roots fulfill the implicit equation for the angle ϑ_α,

$$\cos^2 \vartheta_\alpha = \frac{3r_\alpha + 2L\cos\vartheta_\alpha}{3r_\alpha \left[M/(LF)\cot\vartheta_\alpha + 1 \right]} - 1 \quad . \quad (12)$$
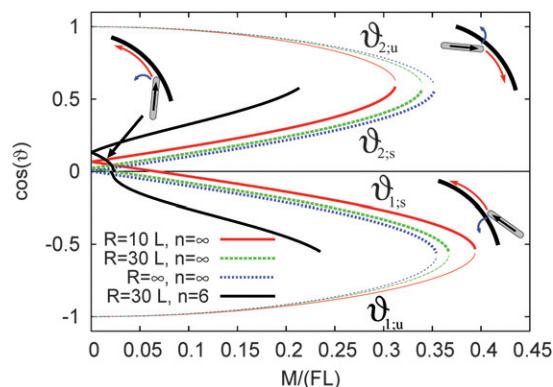
Fig. 2 The stable and the unstable solutions to the steady-state eqn (11) for the angle ϑ for different radii of the circular confinement R_1 or R_2, which are both denoted by R, in the case of hard ($n = \infty$) and soft ($n = 6$) walls. The steady-state angles are denoted by (from top to bottom) $\vartheta_{2;u}$ (unstable, outer wall), $\vartheta_{2;s}$ (stable, outer wall), $\vartheta_{1;s}$ (stable, inner wall if $\cos\vartheta_{1;s} < 0$ and outer wall if $\cos\vartheta_{1;s} > 0$), and $\vartheta_{1;u}$ (stable, outer wall), respectively. The different stable modes are sketched in the pictograms.

Here,

$$r_\alpha = R - (L/2)\cos\vartheta_\alpha \qquad (13)$$

is the position of the rod center of mass in the steady state, i.e., the front rod tip is situated right at the radial position of the inner or outer wall, $R = R_1, R_2$. For simplicity, we denote the radius of the inner *and* outer wall here by R; this is justified because $V(r, \vartheta)$ in eqn (8) is symmetric under interchange of R_1 and R_2. Whether R refers to the inner or outer radius depends on the sign of $\cos\vartheta_\alpha$: If $\cos\vartheta_\alpha > 0$, then $r_\alpha < R$ and R corresponds to the outer wall; if $\cos\vartheta_\alpha < 0$, the opposite is the case.

The solutions to eqn (12) as a function of the positive torque-to-force ratio $M/(LF)$ for different values of R are plotted in Fig. 2. Upon change of the sign of $M/(LF)$, also the sliding angle ϑ_α changes sign. However, the value of $\cos\vartheta_\alpha$ is clearly independent of whether $M/(LF)$ is positive or negative. The upper two branches in Fig. 2, which are characterized by a positive value of $\cos\vartheta_\alpha > 0$, describe the two sliding modes at the outer wall. The lower two branches describe the respective modes at the inner wall, as long as $\cos\vartheta_\alpha < 0$. For small torque-to-force ratios, however, if the swimmer's intrinsic radius $R_0 = (2/3)L^2F/M$ is larger than the radius of the inner confining wall R_1, i.e., if $M/(LF) < (2/3)L/R_1$, the upper of the two lower branches is positive (i.e., $\cos\vartheta_\alpha > 0$). In this regime, which is discussed in detail further down, there is only one mode at the inner wall.

In the case of intermediate but not too large torque-to-force ratios it turns out that for each of the walls there is a stable and an unstable solution to the steady-state conditions: The two central branches with the smaller absolute values of $|\cos\vartheta_\alpha|$ describe the stable modes whereas the outer branches describe the unstable modes. The latter are characterized by the observation that a small fluctuation in the swimmer's coordinates $\mathbf{r}$ or ϑ leads away from the unstable solution. Depending on the width of the channel $R_2 - R_1$ with respect to the swimmer's intrinsic radius R_0, the fluctuation leads the swimmer coordinate either to a neighboring stable branch at the same or opposite wall, or to the central region of the confining ring, where the swimmer might not find another stable sliding mode. The stable modes, on the contrary, are robust against small disturbances. Large fluctuations, however, might make the swimmer leave one stable mode in favor of a neighbouring, other stable mode.

We denote the angles, which correspond to the different branches in Fig. 2 (from top to bottom), by $\vartheta_{2;u}$ (unstable, outer wall), $\vartheta_{2;s}$ (stable, outer wall), $\vartheta_{1;s}$ (stable, inner wall), and $\vartheta_{1;u}$ (stable, outer wall), respectively, where the numbers refer to the two radii R_1 and R_2 and the subscripts "u" and "s" to the unstable and stable modes.

In the limit of large radii $R_{1,2} \gg L$ the ring-like confinement locally resembles a linear channel and the upper and the lower two solutions to eqn (12) become mirror-symmetric about $\cos\vartheta = 0$. Furthermore, the four solutions to the steady-state conditions can then be given analytically, as was already presented in ref. 28:

$$\cos\vartheta_{1,2;s,u} = \mp\sqrt{\frac{1 - 2\left(\frac{M}{LF}\right)^2 \mp \sqrt{1 - 8\left(\frac{M}{LF}\right)^2}}{2 + 2\left(\frac{M}{LF}\right)^2}} \; . \qquad (14)$$

Here, the minus sign in front of the outer square root corresponds to the two modes at the inner wall, whereas the plus sign describes the two modes at the outer wall. The minus sign in front of the inner square root corresponds to the stable and the plus sign to the unstable solution. The solutions, eqn (12), are plotted in Fig. 2.

If the torque-to-force ratio exceeds an R- and wall-dependent critical value, $M/(LF) > \xi_i(R_i)$, $i = 1, 2$, there is no solution to the steady-state conditions; instead, the rod keeps on rotating, whenever it hits one of the walls. The indices 1 and 2 refer to the inner and outer walls, respectively. In the case of a linear channel or a ring-like confinement of diverging radii R_1 and R_2, the critical torque-to-force ratio is determined by a vanishing inner square root in eqn (14). It is thus given by

$$\xi = (2\sqrt{2})^{-1} \approx 0.35 \; . \qquad (15)$$

For a ring-shaped confinement of finite radii, the limiting torque-to-force ratios of stability at the inner and the outer walls depart from the analytical solutions, eqn (15). For large radii, we found numerically that the difference of the limiting values $\xi_i(R_i) - \xi$ displays a power-law behaviour as a function of R_i; in particular,

$$\xi_i(R_i) - \xi \simeq \pm C/R_i \; , \qquad (16)$$

where $C \approx 0.41$ is a common prefactor to both limiting values at the inner and the outer walls. In eqn (16), the plus sign corresponds to the limit of stability at the outer wall ξ_2 (i.e., the limit of the lower two branches in Fig. 2) and the minus sign to the limit of stability at the inner wall ξ_1 (i.e., the limit of the upper two branches in Fig. 2).

In the region of small $M/(LF) < (2/3)L/R_i$, $i = 1, 2$, the behaviour at the inner and the outer walls is qualitatively different: At the inner wall, the stable solution to the steady-state conditions disappears, if the swimmer's intrinsic radius $R_0 = (2/3)L^2F/M$ is larger than the radius of the inner confining wall R_1, i.e., if $M/(LF) < (2/3)L/R_1$. At the outer wall, in contrast, there appears a second stable solution in the same regime of torque-to-force ratios, i.e., if $M/(LF) < (2/3)L/R_2$. In this second branch, the swimmer rotates clockwise, i.e., $\dot\theta > 0$, instead of counter-clockwise, as in the other stable and unstable modes. Since the sliding mode at the outer wall is still described by the same branch in Fig. 2, which describes the sliding mode at the inner wall for larger torque-to-force ratios, we denote it by the same variable $\vartheta_{1;s}$.

The angular velocities corresponding to the stable sliding modes are given by

$$\Omega_{i;s} = v_{i;s}/r_{i;s} \; ,$$
$$v_{i;s} = \frac{\beta D_\parallel F}{2}\frac{\sin\vartheta_{i;s}}{1 + \cos^2\vartheta_{i;s}} \; . \quad i = 1, 2 \; . \qquad (17)$$

This is formally the same result as for a linear channel.[28] A summary about the properties of the stable sliding modes in ring-like confinement for positive torque-to-force ratios is given in Table 1. In the case of a dish-like confinement, which is formally characterized by a vanishing radius $R_1 = 0$, the sliding mode at the inner wall disappears.

Table 1 Characterisation of the stable sliding modes in ring-like confinement: Denoted are the ranges of the angles of stability $\vartheta_{i;s}$, the ranges of torque-to-force ratios $M/(LF)$, the walls, at which the sliding modes are present, and the sign of the corresponding angular velocity $\Omega_{i;s}$

Angle	Stability range	Wall	Velocity
$-\frac{\pi}{4} < \vartheta_{1;s} < 0$	$\frac{2L}{3R_1} < \frac{M}{LF} < \xi_1$	inner	$\Omega_{1;s} > 0$
$\frac{\pi}{4} < \vartheta_{2;s} < \frac{\pi}{2}$	$0 < \frac{M}{LF} < \xi_2$	outer	$\Omega_{2;s} < 0$
$0 < \vartheta_{1;s} < \frac{\pi}{4}$	$0 < \frac{M}{LF} < \frac{2L}{3R_2}$	outer	$\Omega_{1;s} > 0$

In summary, we found that a counter-clockwise circle swimmer can swim clockwise if it is situated in the stable sliding mode characterized by the angle $\vartheta_{2;s}$. It turns out, that this sliding mode is highly relevant for the stochastic swimmer in confinement, which is discussed in the following section.

For large but finite exponents n, the stable and unstable modes change their quantitative values. The qualitative features are the same, as seen for $n = 6$ in Fig. 2 as well.

IV. Stochastic motion at finite temperature

If noise is turned on, the swimmer eventually leaves one of the stable sliding modes and tumbles in between the two confining walls until it reaches the original or the opposite wall under an appropriate angle for the respective sliding mode. However, before we discuss the intricate effects of the two walls in the presence of noise on the swimmer's long-time motion, we shortly recall the properties of the free swimmer in the bulk, which have been discussed at length in ref. 28: For finite temperature all moments of $\mathbf{r}$ and ϕ can be calculated exactly. The first and second moments of $\phi(t)$ are simply given by

$$\bar{\phi} = \phi_0 + \omega_0 t , \qquad (18)$$

$$\overline{\Delta\phi^2} = \overline{[\phi(t) - \phi_0]^2} = (\omega_0 t)^2 + 2D_r t , \qquad (19)$$

where $\phi_0 = \phi(t = 0)$, and where we let ϕ run *ad infinitum*. The first and second moments of $\Delta\mathbf{r} \equiv \mathbf{r}(t) - \mathbf{r}(0)$ are given by

$$\overline{\Delta\mathbf{r}} = \lambda\left[D_r\hat{u}_0 + \omega_0\hat{u}_0^\perp - e^{-D_r t}\left(D_r\bar{\hat{u}} + \omega_0\bar{\hat{u}}^\perp\right)\right],$$

$$\overline{\Delta\mathbf{r}^2} = 2\lambda^2\left\{\omega_0^2 - D_r^2 + D_r\left(D_r^2 + \omega_0^2\right)t\right.$$
$$\left. + e^{-D_r t}\left[\left(D_r^2 - \omega_0^2\right)\cos(\omega_0 t) - 2D_r\omega_0\sin(\omega_0 t)\right]\right\}$$
$$+ 2\left(D_\parallel + D_\perp\right)t, \qquad (20)$$

with $\lambda = \beta D_\parallel F/(D_r^2 + \omega_0^2)$, $\hat{u}_0 = (\cos\phi_0, \sin\phi_0)$, $\hat{u}_0^\perp = (-\sin\phi_0, \cos\phi_0)$, $\bar{\hat{u}} = (\cos\bar{\phi}, \sin\bar{\phi})$, and $\bar{\hat{u}}^\perp = (-\sin\bar{\phi}, \cos\bar{\phi})$, *i.e.*, $\overline{\Delta\mathbf{r}}$ describes an exponentially damped circular trajectory with a damping constant of the short-time rotational diffusion constant D_r, which is referred to as a *spira mirabilis*. In Fig. 3, $\overline{\Delta\mathbf{r}}$ is plotted for $\beta FL = 60$ and $\beta M = 5$, which according to eqn (9) yields an
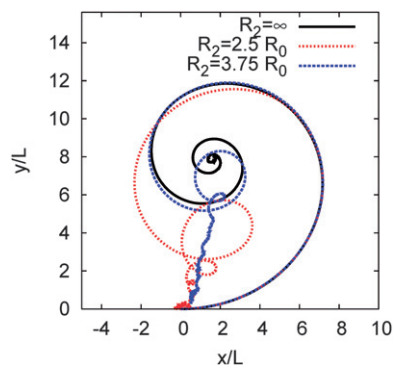

Fig. 3 Trajectories of the mean position $\bar{\mathbf{r}}$ of the self-propelled rod for fixed $\beta FL = 60$ and $\beta M = 5$ ($\mathbf{r}_0 = \mathbf{0}$, $\phi_0 = 0$), yielding an intrinsic radius of $R_0 = 8L$, in dish-like confinements of different radii $R_2/R_0 = 2.5, 3.75$, which is compared to the mean trajectory in the bulk ($\beta V = 0$ or $R_2/R_0 = \infty$).

intrinsic radius of curvature $R_0 = 8L$. The long-time motion of the swimmer in the bulk is diffusive with a diffusion constant

$$D_L \equiv \lim_{t \to \infty}\frac{\overline{\Delta\mathbf{r}^2}}{4t} = \frac{\left(\beta D_\parallel F\right)^2 D_r}{2\left(D_r^2 + \omega_0^2\right)} + \frac{1}{2}\left(D_\parallel + D_\perp\right) . \qquad (21)$$

The stochastic motion of the swimmer in dish- and ring-like confinement has been analyzed by means of extensive Brownian dynamics computer simulations.[33] The equations of motion (1) and (2) were integrated *via* Ermak's algorithm,[34,33] with a timestep $\Delta\tau = 10^{-5}\tau_B$. The power-law exponent in eqn (8) has been set $n = 6$ in all studies. Typical trajectories for the cases of the ring- and the dish-like confinements are shown in Fig. 4(a) and (b) for parameters $\beta FL = 60$, $\beta M = 5$, $R_2 = 30L$, and $R_1 = 0$ (dish) or $R_1 = 15$ (ring), respectively. In these examples, the intrinsic radius $R_0 = 8L$ is significantly smaller than the confining radii R_1 and R_2.

A. Petri dish-like confinement

We first consider the situation of a dish-like confinement ($R_1 = 0$) with a (outer) confining radius R_2, which is larger than the
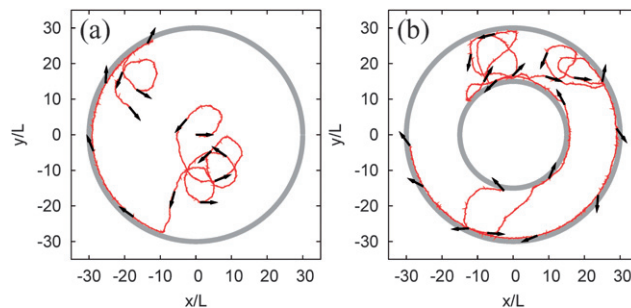

Fig. 4 Typical trajectories of the rod for $\beta FL = 60$, $\beta M = 5$ (yielding an intrinsic radius $R_0 = 8L$), in dish-like confinement of radii $R_1 = 0$ and $R_2 = 30L$ (a) and ring-like confinement of radii $R_1 = 15L$ and $R_2 = 30L$ (b), respectively, for times $0 < t < 5\tau_B$ in (a) and $0 < t < 7\tau_B$ in (b). In (a) the swimmer starts moving at the center at $\mathbf{r}_0 = \mathbf{0}$ with an orientation $\phi_0 = 0$. In (b) the swimmer is initially situated at a random position between the two confining walls.

intrinsic radius of the swimmer, *i.e.*, $R_2 > R_0$. Furthermore, we consider the situation in which the swimmer starts moving at the center at $\mathbf{r}_0 = \mathbf{0}$ with an orientation $\phi_0 = 0$. As is illustrated by the trajectory in Fig. 4(a), the swimmer behaves as in the bulk for short times: It performs circular motion, which is only disturbed by the stochastic force $\mathbf{f}$ and the torque τ, respectively. On times $t \gtrsim D_r^{-1}$ the motion becomes diffusive, as is also reflected in the mean-square displacement $\overline{\Delta \mathbf{r}^2}$ of the swimmer in the bulk, which displays a crossover from an oscillatory ballistic to a diffusive regime at $t = D_r^{-1}$ [see eqn (20)]. The confining wall is typically reached by diffusion at a characteristic time $t \approx R_2^2/(4D_L)$, which, in the limit of large forces $\beta FL \gg 1$, scales as $R_2^2/(4D_L) \propto R_2^2(D_r^2 + \omega_0^2)/F^2$. Once the swimmer hits the confining wall, it might get trapped in the stable sliding mode characterized by $\vartheta_{2;s}$ (see Fig. 2 and Table 1 for the qualitatively same features of the respective mode in hard-wall confinement), which forces the particle to move in a clockwise fashion along the confining wall, against its intrinsic spin (see Fig. 4(a) for a sample trajectory). Different from the deterministic situation, the swimmer might leave the stable sliding mode after a while due to the presence of noise. How often the swimmer leaves the wall depends on the stability of the sliding mode.

In the following, we restrict our consideration to a swimmer of constant force $\beta FL = 60$ and different torques in a dish of radius $R_2 = 30L$. For a discussion of different forces and radii see section V. The swimmer's motion is analysed by considering the following average quantities:

(i) Contrary to the situation in the bulk, the mean center-of-mass position of the swimmer in confinement approaches the center of the confining dish at long times, $\lim_{t \to \infty} \bar{\mathbf{r}} = \mathbf{0}$, because the angular coordinate of the swimmer's position θ is uniformly distributed at long times. This is reflected in the mean trajectories for different confinement radii in Fig. 3. As expected, the smaller the confining dish, the earlier the mean trajectory departs from the mean trajectory in the bulk.

(ii) Although the mean position of the swimmer at long times is at the center, the swimmer is very often–for not too large torque-to-force ratios–not located in the middle of the dish but at the wall, which is attributed to the stability of the sliding mode. This is reflected in the enhanced probability density $\rho(x \lesssim R_2)$ to find the radial coordinate of the swimmer's center of mass $r(t)$ close to the confining wall at R_2. The radial probability density is given by

$$\rho(x) = \int\limits_0^{2\pi} d\alpha \rho(x, \alpha), \qquad (22)$$

where

$$\rho(x, \alpha) = \lim_{t \to \infty} \frac{\overline{\delta\big(x - r(t)\big)\delta(\alpha - \vartheta(t)\big)}}{2\pi x} \qquad (23)$$

where

$$\rho(x, \alpha) = \lim_{t \to \infty} \frac{\overline{\delta(x - r(t))\bar{\delta}(\alpha - \vartheta(t))}}{2\pi x} \qquad (23)$$

is the joint radial and angular stationary probability density. $\rho(x)$ is displayed as a function of x for three different torque-to-force ratios in Fig. 5. In particular, ρ is nearly constant throughout the confining dish except in the vicinity of the wall. For the three
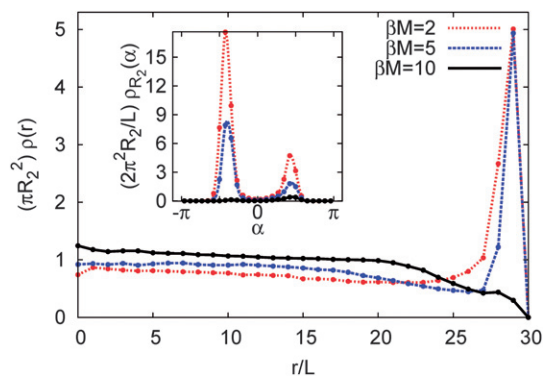

Fig. 5 The probability density $\rho(x)$ of the swimmer in dish-like confinement of radius $R_2 = 30L$, with an internal force $\beta FL = 60$, and for different torques $\beta M = 2, 5, 10$. Inset: The conditional probability $\rho_{R2}(\alpha)$ (for the definition see the main text) for the same parameters.

parameter sets considered in Fig. 5 (all with $\beta FL = 60$ and $R_2 = 30L$) it is observed that the probability to find the particle at the wall, $\rho(x \lesssim R_2)$, decreases with increasing torque: Whereas the torques $\beta M = 2$ and $\beta M = 5$ lead to an enhanced probability at the wall as compared to the central region of the dish, the scenario is inverse in the case of a torque of $\beta M = 10$.

The decrease of the probability with increasing ratio $M/(LF)$ is understood by noticing that the stability of the sliding mode decreases with a decreasing difference of the steady-state angles of the stable and the unstable modes at the wall, $|\vartheta_{2;s} - \vartheta_{2;ul}|$, which are displayed in Fig. 2 for hard walls. For soft walls with an exponent $n = 6$ used in the simulations, the respective values are smaller but the scenario is qualitatively the same. This functional dependence was motivated in the case of a planar wall in ref. 28 [there, it is reflected in the increasing rate of the "flipping" process (a)] and is expected to hold also in the case of a curved wall. That the particle is situated in its stable sliding mode for not too large values of $M/(LF)$ is also reflected in the conditional angular probability density close to the wall,

$$\rho_{R_2}(\alpha) = \int\limits_{R_2 - L}^{R_2} dx \, x \, \rho(x, \alpha), \qquad (24)$$

which is plotted in the inset of Fig. 5. $\rho_{R_2}(\alpha)$ displays a pronounced global maximum at the position of the negative steady-state angle $\vartheta_{2;s} < 0$ in the cases of $\beta M = 2, 5$. The second maximum at $\vartheta \approx -\vartheta_{2;s} > 0$ is attributed to the transient dynamics of an escape event after leaving the stable mode or after hitting the wall under an angle, which is inappropriate for getting trapped in the stable sliding mode. For the larger torque of $\beta M = 10$, the otherwise secondary maximum becomes the global maximum. Apparently, the deterministically stable mode $\vartheta_{2;s}(M/(LF) = 0.167)$ (see Fig. 2) is easily escaped by the swimmer due to thermal fluctuations.

(iii) The stable sliding mode at the confining wall eventually leads to a negative mean angular velocity at long times, which we refer to as the lap frequency (referring to the number of laps/rounds the swimmer's center of mass undergoes per time)

$$\Omega \equiv \lim_{t \to \infty} \overline{\dot{\theta}(t)}. \qquad (25)$$

The lap frequency and the angular diffusion constant,

$$D_\Omega = \lim_{t \to \infty} \frac{\overline{(\theta(t) - \Omega t)^2}}{2t} \quad , \qquad (26)$$

are plotted as a function of the torque-to-force ratio $M/(LF)$ for the same constant force $\beta FL = 60$ and the same confining radius $R_2 = 30L$, as already considered before, in Fig. 6. $\Omega(M/(LF))$ is compared to the lap frequency obtained in the absence of thermal noise, which we discuss at first as a reference case. In this situation–under appropriate initial conditions–the swimmer orientation adopts the value of the stable sliding mode $\vartheta_{2;s}$ for torque-to-force ratios smaller than the critical value $\xi_2(R_2)$. The latter critical value is given by eqn (16) for hard walls and is slightly smaller for soft walls, as seen in Fig. 1. According to eqn (17) the velocity along the channel is an increasing function of the angle $\vartheta_{2;s}$ in the case of hard walls; this behaviour is preserved in the case of soft walls and reflected in the decreasing absolute value of Ω as a function of torque-to-force ratio in Fig. 6. Apart from the lap frequency we also measured the mean angular velocity of the swimmer orientation,
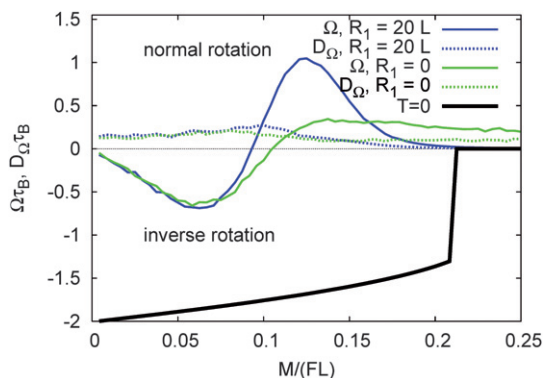

Fig. 6 The lap frequency Ω as a function of $M/(LF)$ in dish- and ring-like confinements for the same parameters as in Fig. 4. The lap frequencies of the stochastic swimmer in dish-like (dotted curve, black) and ring-like (dashed curve, red) confinement are compared to the deterministic situation (solid curve, black) of a swimmer in dish-like confinement, which is given by eqn (17).
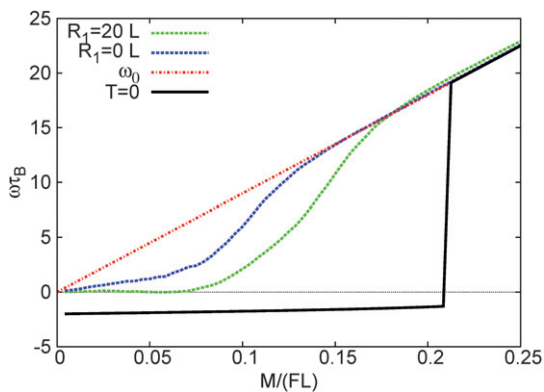

Fig. 7 The spinning frequency ω as a function of $M/(LF)$ for the same parameters as in Fig. 6. Also plotted is the intrinsic spinning frequency ω_0.

$$\omega = \lim_{t \to \infty} \overline{\dot{\phi}(t)} \quad , \qquad (27)$$

which is referred to as the mean spinning frequency and plotted as a function of the torque-to-force ratio in Fig. 7. In the case of zero noise, the spinning frequency is identical to the lap frequency for torque-to-force ratios smaller than the critical value, $M/(LF) < \xi_2(R_2)$. Beyond this value, ω jumps discontinuously to a high, positive value of the intrinsic spinning frequency ω_0 given by eqn (10).

The situation at a finite temperature is significantly more complex: The lap frequency displays a non-monotonous behaviour as a function of $M/(LF)$. This behaviour is attributed to a subtle interplay of the stability of the sliding mode, which yields a clockwise circular motion, and the favoured, intrinsic counterclockwise rotation.

For zero torque the net angular velocity is zero for symmetry reasons. The presence of the stable sliding modes in the positive and the negative angular directions is here reflected by the large amplitude of the angular diffusion constant D_Ω, which is also displayed in Fig. 6. With increasing torque-to-force ratio, the sliding mode in the clockwise direction (the upper (stable) branch in Fig. 2, displaying $\cos \vartheta_{2;s}$) becomes more stable than the sliding mode in the counter-clockwise direction. Moreover, the latter sliding mode becomes extinct once the corresponding branch for $\cos \vartheta_{1;s}$ in Fig. 2 becomes negative. The stability of the mode characterized by $\vartheta_{2;s}$ is therefore responsible for the negative lap frequency $\Omega < 0$.

Beyond a parameter-dependent torque-to-force ratio, the absolute value $|\Omega|$ decreases and a different effect comes into play: Whenever the particle detaches from the wall, it may either quickly find the stable sliding mode again, or it might move away from the wall towards the central region of the dish by diffusion. The latter behaviour is increasingly frequent with increasing ratio $M/(LF)$. Eventually, the swimmer "freely" circles the center of the confining dish, which then gives a positive contribution to the lap frequency Ω. With increasing torque-to-force ratio the number of rounds in the counter-clockwise direction around the center of the dish increases, because the rate of detachment from the stable sliding mode increases. At an intermediate, parameter-dependent ratio $M/(LF)$ the lap frequency changes sign and the counter-clockwise rotational motion become dominant. However, once the area of the mean surrounded circle is significantly smaller than the area of the dish, circling the center of the dish is less likely. Instead, the swimmer performs free circular motion off-center, which does not contribute to the lap frequency. For large $M/(LF)$, the distorting effect of the confining wall becomes negligible, which is reflected in an undisturbed spinning frequency $\omega \simeq \omega_0$ (see Fig. 7). Therefore, Ω can in this regime be estimated by

$$\Omega \approx \omega_0 (R_0/R_2)^2 = \frac{2\beta D_\parallel FL}{3R_2^2} \left(\frac{M}{FL} \right)^{-1} \quad , \qquad (28)$$

where we assumed the fraction of time, during which the swimmer circles the center, to be given by the fraction of the area encircled by the swimmer over the area of the dish. In particular, Ω slowly decays as $1/M$. Quantitatively, the estimated velocity is roughly a factor of ~ 1.2 higher than the velocities obtained from the simulations for $M/(LF) > 0.15$ and the internal force and confining radius considered.

While Ω is a decreasing function of $M/(LF)$, the diffusion constant D_Ω is almost constant throughout the regime of $0.15 \lesssim M/(LF) \lesssim 0.25$. This behaviour is attribute to the increasing rareness of situations, in which the swimmer is situated at the middle of the dish, whereas the number of rounds performed by the swimmer, once situated in the middle, is still significantly high. The diffusion constant can be estimated from a simple two-state model

$$\dot{\theta} = \omega_0 u , \qquad (29)$$

where u is a random variable, which takes the two values $u = 0$ or $u = 1$. Whenever the swimmer is in the center, we attribute to it an angular velocity of $\dot{\theta} = \omega_0$ (implying $u = 1$), whereas we assume the angular velocity to be zero in all other cases. The stationary probability distribution of the random variable u within this simplified picture is therefore given by

$$P(u) = (1 - \Omega/\omega_0)\delta(u) + (\Omega/\omega_0)\delta(1 - u) . \qquad (30)$$

This distribution apparently yields the mean velocity $\bar{\dot{\theta}} = \Omega$. In order to obtain the angular diffusion constant, we make a simple assumption about the temporal correlations of u: The typical time the swimmer contributes to a finite lap frequency is given by the time $\tau_0 \approx R_0^2/(4D_L)$, it needs to diffuse the distance R_0. We therefore make the intuitive ansatz for the conditional probability density

$$P(u|u') = e^{-|t-t'|/\tau_0}\delta(u - u') + (1 - e^{-|t-t'|/\tau_0})P(u) , \qquad (31)$$

where $u = u(t)$, $u' = u(t')$. Eqns (30) and (31) yield the correlation function

$$\overline{uu'} = (\Omega/\omega_0)\left[\left(1 - \Omega/\omega_0\right)e^{-|t-t'|/\tau_0} + \Omega/\omega_0\right] . \qquad (32)$$

By integration of eqn (29) we thus obtain the desired diffusion constant

$$D_\Omega = \omega_0^2\tau_0(\Omega/\omega_0)(1 - \Omega/\omega_0)/2 . \qquad (33)$$

For the parameters under study, $\beta FL = 60$, $R_2 = 30L$, this simple theory predicts a very slow decrease of the diffusivity in the considered torque-to-force regime in agreement with computer simulations ($D_\Omega(M/(LF) = 0.15) = 0.63$ and $D_\Omega(M/(LF) = 0.25) = 0.58$). However, the theory overestimates the diffusivity obtained from the simulations by a factor of ~ 12 in this regime, which is attributed to an overestimated residence time τ_0: The simple diffusion time of an effective Brownian particle with diffusivity D_L from the center of a circle with radius R_0 to its boundary should be replaced by the averaged mean first-passage time[35] to reach the boundary, averaged over all equally distributed initial positions $\mathbf{r}_0$ inside the circle, *i.e.*, fulfilling $|\mathbf{r}_0| < R_0$. Although we did not calculate this time scale, we expect it to be significantly smaller than the time scale τ_0 considered above, because initial positions close to the boundary contribute strongly with relatively short first passage times.

B. Ring-like confinement

By introducing an inner confining wall with a finite radius $R_1 > 0$, the swimmer obtains the possibility to slide efficiently along both the outer and the inner wall: For a positive torque $M > 0$, which we have assumed during the course of this paper, it slides counter-clockwise along the inner wall, *i.e.*, in positive angular direction, and clockwise along the outer wall, *i.e.*, in negative angular direction, as before. (The steady-state sliding modes in the noise-free case were discussed at length in Section III.)

We now discuss the qualitative differences of the swimmer at finite temperature in a ring-like confinement as compared to the situation in a dish-like confinement. As in the previous subsection, we therefore measured the radial probability density $\rho(x)$ [eqn (22)], the angular velocity Ω [eqn (25)], the angular diffusion constant D_Ω [eqn (26)], and the spinning frequency $\omega = \dot{\phi}$ [eqn (27)]. The short-time dynamics is not examined, as it is strongly dependent on the initial conditions. Here, we only consider a swimmer of constant force $\beta FL = 60$ and different torques in a ring-like confinement of radii $R_1 = 15L$ and $R_2 = 30L$. For a discussion of different forces and radii see section V.

(i) The radial probability density $\rho(x)$ for a confinement of $R_1 = 15L$ and $R_2 = 30L$ is plotted in Fig. 8 for the same force $\beta FL = 60$ and the same three different torques $\beta M = 2, 5, 10$ as examined in the dish-like confinement of the same outer radius $R_2 = 30L$ in Fig. 5. Clearly, the same qualitative features are observed at the outer wall for the dish and the ring. At the inner wall, however, the swimmer behaves qualitatively different as compared to the outer wall: Apparently, the probability of finding the swimmer close the inner wall, $\rho(x \gtrsim R_1)$, is a non-monotonic function of the torque. The probability is large for an intermediate torque, whereas it is small for small and large torques. The non-monotonicity is attributed to a lower stability of the respective sliding mode at the inner wall, which is characterized by the sliding angle $\vartheta_{1;s}$. Different from the situation at the outer wall, the stable sliding mode at the inner wall is lost for torque-to-force ratios smaller than a critical value, which is $M/(LF) < (2/3)L/R_1$ in the case of hard walls, according to Table 1 and slightly different for soft walls, as seen in Fig. 2. For the sample parameters of Fig. 8 the lowermost torque $\beta M = 2$ corresponds to a ratio below the stability limit, *i.e.*, the stable mode is lost. Correspondingly, the probability to find the particle at the inner wall is substantially smaller than at the outer wall. For the intermediate torque $\beta M = 5$, the asymmetry of the radial probabilities is substantially weaker, and at the torque $\beta M = 10$, the situation is inverse, *i.e.*, the particle is much more likely
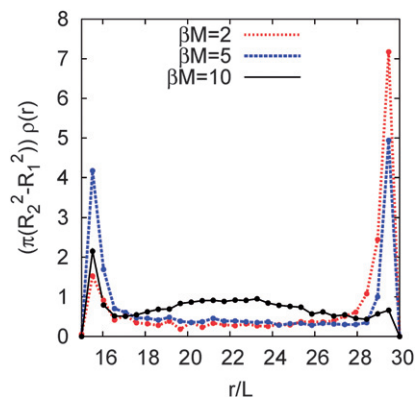

Fig. 8 The radial probability density $\rho(x)$ of the swimmer in ring-like confinement of radii $R_1 = 15L$, $R_2 = 30L$, with an internal force $\beta FL = 60$, and for different torques $\beta M = 2, 5, 10$.

found at the inner than at the outer wall. In this situation, the stability at the outer wall might be lost whereas the sliding mode at the inner wall is still stable, equivalently to the situation in a ring of hard walls according to eqn (16) and Fig. 2.

(ii) The presence of a stable sliding mode at the inner wall is also reflected in a larger lap frequency Ω, which is plotted as a function of the torque-to-force ratio in Fig. 6 for the same force $\beta FL = 60$ and confinement radii $R_1 = 15L$, $R_2 = 30L$ as examined in Fig. 8. In the regime of small torque-to-force ratios, $M/(LF) \lesssim 0.08$, where the sliding mode at the outer wall dominates the swimmer's motion, the lap frequencies in dish- and ring-like confinement agree almost perfectly. Once counter-clockwise motion away from the outer wall becomes more frequent, however, the scenarios are different in the dish and the ring: Whereas a positive lap frequency in the dish comes about by free circular motion of the swimmer around the central point of the dish, the swimmer in the ring exploits the sliding mode $\vartheta_{1;s}$ to efficiently slide in negative angular direction. This qualitative difference is reflected in the different spinning frequencies ω, which are plotted as a function of $M/(LF)$ in Fig. 7: The spinning frequency of the swimmer in the dish is almost equal to ω_0 for torque-to-force ratios $M/(LF) \gtrsim 0.12$, whereas this is the case for the swimmer in the ring only for $M/(LF) \gtrsim 0.16$.

Although it takes the swimmer longer to undergo one round around the center of the ring-like confinement than to undergo one free circle in the dish, the resulting positive lap frequency at an optimum torque-to-force ratio $M/(LF) \approx 0.12$ in the ring is by a factor of $\sim$4 larger than the respective lap frequency in the dish. For the parameter set under study this pronounced difference is due to the fact, that the free swimmer in the dish might either not circle the center of the dish, if $2R_0 < R_2$, or it might diffuse towards the outer wall where it can get trapped in the sliding mode of the outer wall, whereas in the ring, the swimmer is eventually attached to the inner wall for a long time undergoing persistent clockwise rotational motion. As expected, the long-time diffusion constant D_Ω displays a peak at $M/(LF) \approx 0.1$, where Ω is almost zero. However, the peak is not very high as compared to the diffusivity at zero torque.

Beyond its peak position, the lap frequency Ω decreases much faster with increasing torque-to-force ratio as in the dish, simply due to the fact that the particle cannot freely circle the center of the confinement in the latter situation. The finite, positive lap frequency for torque-to-force ratios larger than the stability limit $\xi_i(R_i)$, $i = 1, 2$, is reminiscent of the asymmetry in the stability of the two sliding modes, characterized by $\vartheta_{1;s}$ and $\vartheta_{2;s}$, respectively. The angular diffusivity D_Ω also decreases much faster with increasing torque-to-force ratio than in the dish. Clearly, the possibility to freely circle the center of the confinement is lacking in the ring due to the presence of the inner wall. Therefore, diffusion in the ring is governed by free diffusion of the circle-swimming particle in between the two walls and by the distortions of the free motion due to occasional encounters with the walls. In fact, it turns out, that these encounters lead to a decrease of the long-time diffusivity with increasing torque-to-force ratio that is remarkably faster than the decrease of the bulk diffusivity D_L of eqn (21).

V. Conclusions

In conclusion, within a simple model of Brownian dynamics combined with internal and external forces, we have studied the dynamics of a circle swimmer in confining Petri dish- and ring-like circular geometries. Though the circle swimmer has its prescribed intrinsic orientational motion, a cylindrical confinement can invert the orientational sense of the motion. We have shown this by an analytical discussion of the noise-free steady-state motion and by extensive Brownian dynamics computer simulations, which include noise. The dynamics do change qualitatively for increasing torque-to-force ratio: the orientational sense is only inverted if this ratio is small enough.

In the following few paragraphs, we shortly comment on different parameter values from those used up to now, i.e., where $\beta FL \neq 60$, $R_1 \neq 0$, $15L$, and $R_2 \neq 30L$, respectively: For smaller internal forces, at a constant torque-to-force ratio, the stability of the sliding modes decreases. Furthermore, the trajectories of the swimmer in the bulk or in the central region of the dish lose their pronounced circular structure. Both effects are expected to lead to a decrease of the absolute value of the angular velocity $|\Omega|$. Whether the negative peak of Ω at small values of $M/(LF)$, seen in Fig. 6, persists, remains an open question and might also depend on the confinement radii R_1 and R_2. In the case of the dish, the non-monotonicity of Ω was attributed to a subtle competition of the stability of the sliding mode and the probability to surround the center of the dish in the detached situation of free circular motion. The former stability is ruled by an energy scale to surmount an action barrier of detaching from the wall (see the discussion for a planar wall in ref. 28), whereas the latter probability is ruled by the ratio of the length scales R_0 and R_2. Therefore, a loss of the rotational inversion cannot be ruled out for smaller internal forces.

In rings of two confining radii R_1 and R_2 the situation is significantly more complex than in dishes due to the presence of the new length scale R_1. We expect, that the inversion from clockwise to counter-clockwise motion at small torque-to-force ratios is robust to large changes in βFL, R_1, and R_2, respectively, as long as the asymmetry in the stabilities of the two stable sliding modes at both walls is significant. However, the qualitative and quantitative changes of the lap frequency with changing parameters have to be studied in detail and are deferred to a future work.

For larger forces we expect the non-monotonicity of Ω to become more pronounced: Whereas the stability of the sliding mode increases exponentially with the action barrier, which in turn is a linear function of the force for large forces, the probability to circle the center of a dish is only weakly sensitive to the force, once the trajectories of the freely moving swimmer are distinctively circular.

In the case of a dish, we therefore expect the negative peak of Ω at small torque-to-force ratios to broaden and asymptotically reach the deterministic velocity curve $\Omega \simeq \Omega_{2;s}$ of eqn (17), which is a linear function of F (the curve is plotted for $\beta FL = 60$ in Fig. 6 as well). The positive part of Ω is expected to continue to obey eqn (28), which predicts a linear increase with ω_0. Summarizing, the force-normalized velocity profile Ω/F as a function of the torque-to-force ratio is expected to asymptotically approach a universal, F-independent function which is given by

$$\frac{\Omega}{F} \simeq \frac{\Omega_{2;s}}{F} + \Theta\left[M/(LF) - \xi_2(R_2)\right]\left(\frac{R_0}{R_2}\right)^2 \frac{\omega_0}{F} \; , \qquad (34)$$

where $\Theta[x]$ is the Heaviside step function.

Whereas the peak of the positive lap frequency is expected to vanish in the case of a dish, the situation is qualitatively different in the case of a ring. Here, a third regime is expected to persist in between the regimes of the stable sliding mode at the outer wall and free circular motion inbetween the walls: For intermediate torque-to-force ratios, sliding along the inner wall is more stable than along the outer wall. Therefore, the positive peak of Ω is expected to increase up to the value of $\Omega \simeq \Omega_{1;s}$. Beyond $M/(LF) = \xi_1(R_1)$, the swimmer rotates freely and the lap frequency decays rapidly towards zero. Not only the lap frequency but also the diffusivity D_Ω is expected to sharpen with an increasing internal force. In particular, we expect to observe a strong enhancement of the diffusivity in a broad range of torque-to-force ratios, according to a recent study of a simple one-dimensional model system of an overdamped particle with a tilted, bistable potential for the particle velocity, discussed by Lindner and Nicola.[36] According to ref. 36, the diffusivity could be used to quantify the, in this work only qualitatively discussed, asymmetry in the stability of the two sliding modes at the inner and the outer wall, respectively.

Finally, more generally, we remark that our model is a good realization for various "active" soft matter systems. The first are "living" objects like bacteria[4–9,23,24] and spermatozoa[10–12] when exposed to an external substrate together with a further lateral confinement.[5,25] Second, inert colloidal particle and nanorods can be made active by a catalytic reaction at their surface.[14–16] These particles can be confined in microchannels of arbitrary geometry.[26] Even beyond soft matter, there are further possible realizations in vibrated polar granular rods[19] or for pedestrian dynamics in circular confinement.[21]

For comparison with experiments, we give here an estimate of the relevant dimensionless force and torque, which correspond to the motion of flagella-driven *Escherichia coli* bacteria close to a planar surface, as studied by Lauga *et al.*[6] in the case of no further confining boundaries. They found the bacteria (more precisely, a straight-swimming mutant) to swim at velocities of the order of $v \approx 20\ \mu m\,s^{-1}$ along circular trajectories of typical radii of $R_0 \approx 20\ \mu m$. The rod-like bacteria under study can be regarded as spherocylinders of typical dimensions $\approx 2.5 \times 1.5\ \mu m$. Neglecting the boundary effects on the dynamic viscosity of water η (see the discussion of hydrodynamic effects, above), the velocity v and radius R_0 correspond to a typical effective force and torque of $\beta FL \approx 200$ and $\beta M \approx 3.9$ in our model, respectively. These latter values are of the same order of magnitude as the values used in our computer simulation study ($\beta FL = 60$, $\beta M = 5$). In particular, the corresponding force is even larger than the one used in our study, which, according to the above reasoning, should lead to a more stable sliding mode and therefore to a larger lap frequency, if the bacteria were embedded in a confining dish or ring. Dishes or rings of radii in the range of 100 μm could be realized by lithography as demonstrated in the same work of Lauga *et al.*[6]

In the spirit of increasing complexity, it would be interesting to study more complicated geometries of confinement as, *e.g.*, ratchets[25] or various shapes of "fishing net" to catch self-propelled particles. Finally we would like to explore the collective behaviour of many circle swimmers both in bulk and confinement where new clustering and aggregation effects are expected.[37–40] A complete understanding of the individual and collective nonequilibrium dynamics of active particles is highly desirable to construct mixing and sorting devices.

References

1 J. Toner, Y. H. Tu and S. Ramaswamy, *Ann. Phys.*, 2005, **318**, 170.
2 P. Hänggi and F. Marchesoni, *Rev. Mod. Phys.*, 2009, **81**, 387.
3 E. Gauger and H. Stark, *Phys. Rev. E: Stat., Nonlinear, Soft Matter Phys.*, 2006, **74**, 021907.
4 H. C. Berg and L. Turner, *Biophys. J.*, 1990, **58**, 919.
5 W. R. DiLuzio, L. Turner, M. Mayer, P. Garstecki, D. B. Weibel, H. C. Berg and G. M. Whitesides, *Nature*, 2005, **435**, 1271.
6 E. Lauga, W. R. DiLuzio, G. M. Whitesides and H. A. Stone, *Biophys. J.*, 2006, **90**, 400.
7 J. Hill, O. Kalkanci, J. L. McMurry and H. Koser, *Phys. Rev. Lett.*, 2007, **98**, 068101.
8 V. B. Shenoy, D. T. Tambe, A. Prasad and J. A. Theriot, *Proc. Natl. Acad. Sci. U. S. A.*, 2007, **104**, 8229.
9 S. Schmidt, J. van der Gucht, P. M. Biesheuvel, R. Weinkamer, E. Helfer and A. Fery, *Eur. Biophys. J.*, 2008, **37**, 1361.
10 I. H. Riedel, K. Kruse and J. Howard, *Science*, 2005, **309**, 300.
11 D. M. Woolley, *Reproduction*, 2003, **126**, 259.
12 B. M. Friedrich and F. Jülicher, *New J. Phys.*, 2008, **10**, 123025.
13 S. Nakata, Y. Iguchi, S. Ose, M. Kuboyama, T. Ishii and K. Yoshikawa, *Langmuir*, 1997, **13**, 4454.
14 P. Dhar, T. M. Fischer, Y. Wang, T. E. Mallouk, W. F. Paxton and A. Sen, *Nano Lett.*, 2006, **6**, 66.
15 A. Walther and A. H. E. Müller, *Soft Matter*, 2008, **4**, 663.
16 A. Erbe, M. Zientara, L. Baraban, C. Kreidler and P. Leiderer, *J. Phys.: Condens. Matter*, 2008, **20**, 404215.
17 R. Dreyfus, J. Baudry, M. L. Roper, M. Fermigier, H. A. Stone and J. Bibette, *Nature*, 2005, **437**, 862.
18 M. N. Popescu, S. Dietrich and G. Oshanin, *J. Chem. Phys.*, 2009, **130**, 194702.
19 A. Kudrolli, G. Lumay, D. Volfson and L. S. Tsimring, *Phys. Rev. Lett.*, 2008, **100**, 058001.
20 T. Ohta and T. Ohkuma, *Phys. Rev. Lett.*, 2009, **102**, 154101.
21 T. Obata, T. Shimizu, H. Osaki, H. Oshima and H. Hara, *J. Korean Phys. Soc.*, 2005, **46**, 713.
22 J. Elgeti and G. Gompper, *Europhys. Lett.*, 2009, **85**, 38002.
23 G. Li, L.-K. Tam and J. X. Tang, *Proc. Natl. Acad. Sci. U. S. A.*, 2008, **105**, 18355.
24 A. P. Berke, L. Turner, H. C. Berg and E. Lauga, *Phys. Rev. Lett.*, 2008, **101**, 038102.
25 S. E. Hulme, W. R. DiLuzio, S. S. Shevkoplyas, L. Turner, M. Mayer, H. C. Berg and G. M. Whitesides, *Lab Chip*, 2008, **8**, 1888.
26 R. Bubeck, P. Leiderer and C. Bechinger, *Prog. Colloid Polym. Sci.*, 2001, **118**, 73.
27 M. B. Wan, C. J. O. Reichhardt, Z. Nussinov and C. Reichhardt, *Phys. Rev. Lett.*, 2008, **101**, 018102.
28 S. van Teeffelen and H. Löwen, *Phys. Rev. E: Stat., Nonlinear, Soft Matter Phys.*, 2008, **78**, 020101.
29 O. Raz and J. E. Avron, *New J. Phys.*, 2007, **9**, 437.
30 R. Golestanian, T. B. Liverpool and A. Ajdari, *New J. Phys.*, 2007, **9**, 126.
31 R. Golestanian and A. Ajdari, *Phys. Rev. Lett.*, 2008, **100**, 038101.
32 E. R. Dufresne, T. M. Squires, M. P. Brenner and D. G. Grier, *Phys. Rev. Lett.*, 2000, **85**, 3317.
33 M. P. Allen and D. J. Tildesley, *Computer Simulation of Liquids*, Clarendon Press, Oxford, 1987.
34 D. L. Ermak, *J. Chem. Phys.*, 1975, **62**, 4189.
35 H. Risken, *The Fokker–Planck Equation, Methods of Solution and Applications*, Springer, Berlin, 2nd edn, 1989.
36 B. Lindner and E. M. Nicola, *Phys. Rev. Lett.*, 2008, **101**, 190603.
37 R. Kirchhoff and H. Löwen, *Europhys. Lett.*, 2005, **69**, 291.
38 F. Peruani, A. Deutsch and M. Bär, *Phys. Rev. E: Stat., Nonlinear, Soft Matter Phys.*, 2006, **74**, 030904.
39 H. H. Wensink and H. Löwen, *Phys. Rev. E: Stat., Nonlinear, Soft Matter Phys.*, 2008, **78**, 031409.
40 P. Romanczuk, I. D. Couzin and L. Schimansky-Geier, *Phys. Rev. Lett.*, 2009, **102**, 010602.